Indian Journal of Chemical Technology
Vol. 26, January 2019, pp. 9-22

Presentation of anodic electrocatalyst for polymeric fuel cell: Pt nanoparticles immobilized on $NdFeO_3$ nanocrystals and carbon nanotubes

Zahra Yavari*, Meissam Noroozifar & Mozhgan Khorasani-Motlagh
Department of Chemistry, University of Sistan and Baluchestan, P.O Box 98135-674 Zahedan, Iran
E-mail: zahrayavari5@gmail.com

Received 29 June 2016; accepted January 2018

Current catalysts for the methanol oxidation in fuel cells (typically noble metals-based) are susceptible to poisoning with intermediates like CO. Hence superseded catalysts have been desirable for methanol oxidation based on incorporation of mixed oxides. The different types of nanocomposites have been prepared with Pt nanoparticles (PtNPs), functionalized CNTs, perovskite $NdFeO_3$ nanoparticles ($NdFeO_3$NPs) and chitosan (CH) polymer and their catalytic activity toward methanol oxidation have been investigated by the electrochemical studies. The equations of current density versus time are obtained via the fitting and simulation of experimental data. In the following, the amount of transferred charge during methanol oxidation versus time has been calculated through the lower Riemann sum of curve correspond to experimental data and the integration of mentioned equations both. A direct methanol fuel cell (DMFC) is designed, assembled and tested with the suggested PtNPs-CNTs-$NdFeO_3$NPs-CH nanocomposites as an anodic catalyst at variety conditions. The effect of experimental factors on DMFC performances has been investigated and optimized.

Keywords: Transferred charge, Catalytic oxidation, Cyclic voltammetry, Perovskite, Direct methanol fuel cell

The quick reduction of fossil fuel reserves is noticeably forcing governments worldwide to adopt 'Sustainable Models' for energy exploitation. The form of energy most frequently required by man is electricity, which fuel cells are the one device of its production. Direct methanol fuel cells (DMFCs) are extensively considered as clean energy and potentially greatly efficient systems. DMFCs consuming the methanol fuel at liquid form is the potential power sources for wide-ranging applications, for example small electric vehicles, due to its high energy density and low pollution to the environment. The main constituent in a DMFC is the membrane electrode assembly (MEA), and typically it includes a proton exchange membrane with catalyzed electrodes joined to both sides. The selective of nano-size and highly dispersed catalysts to improve the rate of methanol oxidation at the anode side is essential for the efficient performance of DMFC[1]. Usually, noble metals such as Pt[2], Pd[3] and Pt-Ru bimetallic composites[4] are purposed as anodic catalysts for methanol oxidation. The sites of these metals are poisoned by the methanol oxidation intermediates, like CO species formed during the oxidation reaction. Today studies show the applicability of the metal mixed oxides like perovskite as superseded for noble metals in DMFC electrodes[5]. The perovskites have a prominent place in the materials science world because of their favorable characteristics such as structural, ionic as well as electronic conductivity[6], noteworthy thermodynamic stability and the activity of catalytic[7,8]. They can be promising materials for application as the electrode in fuel cells[9], exhaust gas sensors in vehicles[10], membranes for separation processes and above all as catalysts[11-13]. Deshpande *et al.*[14] synthesized a variety of non-noble perovskite substituted noble metal high surface area compounds and evaluated their catalytic activity under DMFC conditions, simultaneously. They found that the perovskites showed better performance comparable with the Pt–Ru catalyst. The $NdFeO_3$ metal oxide is recognized to be orthorhombically distorted perovskite structure. This perovskite has three main magnetic connections inclusive Fe–Fe, Nd–Fe and Nd–Nd. The structural and magnetic properties of $NdFeO_3$ are determined to compete against these interactions[15]. These interesting structural properties and the presence of transition metals with multiple oxidation states lead to applications like gas sensors and electro-catalytic activity. In the other hand, the support nature is most important in catalytic activity, since it controls the dispersion and stability of the composite components, the electronic properties including catalyst-support interactions and also the resistances of mass and

charge transfer of the catalyst[16]. Consequently, special attention is given to the alternative carbon materials among multi-walled carbon nanotubes (CNTs) as catalyst supports for DMFCs[17]. In previous studies, we investigated the electrocatalytic oxidation of methanol on Pt-chitosan (CH)[18] and Pt-functionalized CNTs-CH[19] and reported the addition of chitosan into noble metal-containing catalysts could considerably improve the catalyst performance for methanol oxidation. Chitosan exhibits great advantages due to its non-toxicity and appropriate adhesion in the composite. Diverse approaches to the improvement of an effective, low-cost, multifunctional anodic catalyst for direct methanol-based fuel cells followed.

This study focuses on improving DMFCs performance by suggesting the anodic catalyst with less-loading and less-poisoning noble metals like platinum using CNTs and perovskite oxide in nano-size. To provide more effective reaction sites for the catalysis; $NdFeO_3$ perovskite were synthesized as nano-size particles ($NdFeO_3$NPs). The activity of platinum nanoparticles (PtNPs) in the presence of functionalized CNTs and $NdFeO_3$NPs for methanol oxidation was evaluated using the glassy carbon (GC) electrode. Based on the importance of multifunctional catalysts, incorporating the effect of $NdFeO_3$NPs to PtNPs and CNTs catalyst has been studied for methanol oxidation by electrochemical techniques. For this purpose, PtNPs, PtNPs-$NdFeO_3$NPs and PtNPs-CNTs-$NdFeO_3$NPs nanocomposites with chitosan (CH) polymer as matrix were effectively prepared and then their catalytic activity toward methanol oxidation were compared with each other. The equations of current density versus time were obtained via the fitting and simulation of experimental data. In the following, the amount of transferred charge during methanol oxidation versus time was calculated through the lower Riemann sum of curve correspond to experimental data and the integration of mentioned equations both. The effect of experimental factors on the anodic current density and the potential of methanol oxidation were studied, and the optimum conditions were suggested. Finally, the functions of PtNPs-CNTs-$NdFeO_3$NPs-CH nanocomposites were investigated in the stack and assembled DMFC as anodic catalysts and the polarization curves of single fuel cell were plotted for mentioned DMFC.

Experimental Section

Materials and Instrumentation

The chloride salts of neodymium and ferric, H_2PtCl_6 aqueous solution, octanoic acid and $NaBH_4$ were purchased from Merck Company and used without extra purification.1% Acetic acid (CH_3COOH) solution was prepared with double distilled water (DDW). A natural polymer, Chitosan, ([2-amino-2-deoxy-(1-4)-β-D-glucopyranose]), with a medium molecular weight (about400000 Da) was purchased from Fluka. CNTs with nanotube diameters, *OD* = 20–30 nm, wall thickness = 1–2 nm, length = 0.5–2 μm, and purity > 95% were purchased from Aldrich. The DDW was used to prepare of all solutions. The carbon cloth-diffusion layer (CC-DL) and Nafion117 membrane was purchased from Asian Hydrogen New Science Company (H_2 Engine Company), manufacturing & development Isfahan science and technology town, Isfahan, Iran.

All electrochemical profiles were obtained by a conventional three-electrode cell. A GC electrode with 0.03 cm^2 surface area was used as the working electrode substrate. A platinum electrode and a saturated calomel electrode were employed in the role of the counter and reference electrodes, respectively. All potentials were measured with proportion to this reference electrode. The electrolyte was a mixture of sulfuric acid and the corresponding methanol with an identified concentration. X-ray powder diffraction (XRD) analysis was conducted on a Philips analytical PC-APD X-ray diffractometer along with monochromatic CuK_α radiation (λ = 1.54Å) to characterize the sample. The surface morphology and the sample status were observed with scanning electron microscopy (SEM) (SEM-Philips XL30). The TEM image of the produced nanocomposite was taken by a Philips CM120 transmission electron microscopy with 2.5Å resolution. An air brush kit model MBD-116C was employed to spray the nanocatalyst ink on CC-DL.

Step 1: Synthesis of $NdFeO_3$ nanoparticles

In a typical preparation based on our previous work[20], the 0.1 M solution of ferric chloride ($FeCl_3.6H_2O$) and the 0.1 M solution of neodymium chloride ($NdCl_3.6H_2O$) were mixed for the synthesis of perovskite nanocrystalline. Deionized distilled water was used as the solvent to avoid the impurities production in the product. A known amount of octanoic acid was added to the salt solution as surfactant. The 1.5 M solution of sodium hydroxide (NaOH) was added to the mixture dropwise, slowly. The *p*H of the solution was monitored by adding NaOH solution, constantly. The reactants were stirred until the *p*H was reached the level of 7-8. In the

presence of alkaline NaOH medium, the metal cations were dispersed and formed metal hydroxides in the form of colloidal particles, following Eq. (1):

$$NdCl_3.6H_2O + FeCl_3.6H_2O + 6NaOH \rightarrow Nd(OH)_3.Fe(OH)_3 + 6NaCl + 12H_2O \quad ...(1)$$

The liquid precipitate was brought to a temperature of reaction (~80°C)and stirred for 1 h. After cooling at room temperature, the resulting products were centrifuged for 15 min at 403 RCF and washed with distilled water and ethanol several times to remove the excess surfactant from the solution. The gotten precipitate was dried at 100°C for 5 h. In the next step, to let the burn off the organic compound and product self-ignite in the material, the products were calcinated at 800°C for 5 h. The products were cooled to room temperature, and the neodymium orthoferrite nanoparticles were obtained.

Step 2: Preparation of the nanocomposites

A CH solution (2 $mg.mL^{-1}$) in 1% acetic acid solution (as solvent) has been prepared, because of the poor solubility of the polymer, the mixture was stirred to dissolve entirely and kept 24 h, and the solution was then filtrated to eliminate any impurity. 25 µL of H_2PtCl_6 aqueous solution (0.5 M) was mixed with an identified amount of CH solution using a rotary aperture (100 rpm) for 45 min. CNTs were first subjected to the oxidation operation by vigorously stirring in an acidic mixture (concentrated sulfuric and nitric acid with the volumetric ratio of 3 to 1) at room temperature for 24 h. It is clear that this pre-treatment removes impurities and generates sufficient functional groups on the surface of CNTs. In the following, the treated CNTs were filtered by centrifugation (403RCF) and washed with double distilled water until the *p*H of the filtrate reached 7 and dried at 90°C for 7h. In next step, 1 mg of functionalized CNTs were dispersed into the 0.5 mL of CH solution with stirring, resulting in the uniform carbon ink and was added to the Pt-CH blend and stirred for another 60 min. Afterward, 50 µL of the freshly prepared aqueous solution of 2.5 M $NaBH_4$was added to the mixture as the reducing agent. To completely reduce the Pt ions and obtain the Pt nanoparticles (PtNPs), the blend was kept stirring for 60 min (eq. 2).

$$6NaBH_4 + H_2PtCl_6 \rightarrow Pt + 6NaCl + 3B_2H_6 + 4H_2 \quad ...(2)$$

Then, using an ultrasonic bath, 1 mg $NdFeO_3$NPs was mixed with 0.5 mL CH solution for 30 min ($NdFeO_3$NPs-CH), and this mixture was added to PtNPs-CNTs-CH suspension. Final nanocomposite has been denoted as PtNPs-CNTs-$NdFeO_3$NPs-CH.

Step 3: Electrode preparation

The GC electrode was mechanically polished with 0.05 µm alumina slurry for 3 min to a mirror finish surface and was then rinsed with DDW. It was sonicated in a mixture of water:ethanol (9:1 v/v) for 3 min. Subsequently, the GC electrode was cleaned and activated in an electrochemical cell containing 1 M H_2SO_4 solution by cyclic voltammetry between −1.5 and +1.5 V at a scan rate of 0.1 $V.s^{-1}$ until a stable profile of cyclic voltammetric (≈ 15 times) was obtained. The treated GC electrode was coated by casting 10 µL of the prepared PtNPs-CNTs-$NdFeO_3$NPs-CH suspension, and the electrode was then put under infrared radiation for fast drying (or the electrode was kept for 10 h at room temperature for drying). During this period, the solvent evaporation led to the formation of a deposited nanocatalyst layer on the GC electrode surface. This modified GC electrode has been denoted as GC/PtNPs-CNTs-$NdFeO_3$NPs-CH. Similarly, the same methods have been used for the preparation of GC/PtNPs-CH, GC/$NdFeO_3$NPs-CH, and GC/PtNPs-$NdFeO_3$NPs-CH electrodes.

Step 4: CO stripping investigation

The reaction of CO oxidation on the modified electrodes was evaluated using the CO stripping technique. CO is adsorbed at a constant potential (~ 50 mV) for 15 min. In the following, N_2 gas is purged to remove dissolved CO during 30 min. The potentials scan at 50 $mV.s^{-1}$ were recorded for each of the electrodes.

Step 5: Fuel cell operation

Initially, the prepared suspension nanocatalysts were sprayed uniformly onto CC-DL using the air brush kit. The anode catalyst loading was (2.0 $mg.cm^{-2}$) PtNPs – (1.0 $mg.cm^{-2}$) $NdFeO_3$NPs – (0.6 $mg.cm^{-2}$) functionalized CNTs onto the CC-DL (PtNPs-CNTs-$NdFeO_3$NPs-CH/CC-DL); whiles, the active surface area of the single cell was 5 cm^2. The CC-DL with prepared PtNPs-CH (4 $mg.cm^{-2}$) was used as the cathode. The Nafion117 membrane was pre-treated by successive dipping in 5%wt H_2O_2 solution, double distilled water, 8%wt H_2SO_4 solution and finally in double distilled water again, at 80°C and 30 min each step. The diffusion layers based on carbon cloths with prepared catalyst layers on the

anode and the cathode sides and membrane in the middle were formed the single cell. The anode and cathode layers were hot-pressed onto both sides of the Nafion membrane at 140°C and 200 psi for 4 min. Finally, the membrane electrode assembly (MEA) was cooled down to room temperature and assembled in the single cell for performance evaluation. The flow rate of methanol as fuel was controlled using a peristaltic pump. *I–V* curves were obtained galvanostatically with an electronic load, EL200P, Daegil, and controlled via a personal computer.

Results and Discussion

$NdFeO_3$NPs characterization

Figure 1A shows the XRD pattern of $NdFeO_3$ perovskite. The analysis of XRD pattern was matched to the perovskite-type $NdFeO_3$ (JCPDS File no. 25-2064), which crystallizes in the orthorhombic system with main diffraction peak at d = 2.77 Å ((1 2 1) plane). No peaks attributable to Nd_2O_3 and/or Fe_2O_3 were observed and the initial compound was decomposed to single-phase $NdFeO_3$, entirely. The sharpening of the peaks is due to the high crystallinity of the $NdFeO_3$NPs. The peak broadening confirmations in XRD patterns showed that $NdFeO_3$particles are nano-size. The mean size of the $NdFeO_3$NPs (D) was estimated by XRD line broadening using the Debye-Scherer equation[21]:

$$D = \frac{0.89 \times \lambda}{B \times \cos\theta} \qquad ...(3)$$

λ is the X-ray radiation wavelength (1.54 Å), θ is the Bragg angle and B is the breadth of the observed diffraction line in its half intensity maximum. The mean crystallite size of $NdFeO_3$NPs has obtained 76.08 nm.

The size, structure and morphology of the $NdFeO_3$NPs were considered using SEM (Fig. 1B). The SEM micrograph was approved that the grains were composed of tremendously fine particles and were secondary agglomerates of primary particles. It was observed that nanoparticles started to become evident within the grains and agglomerates and

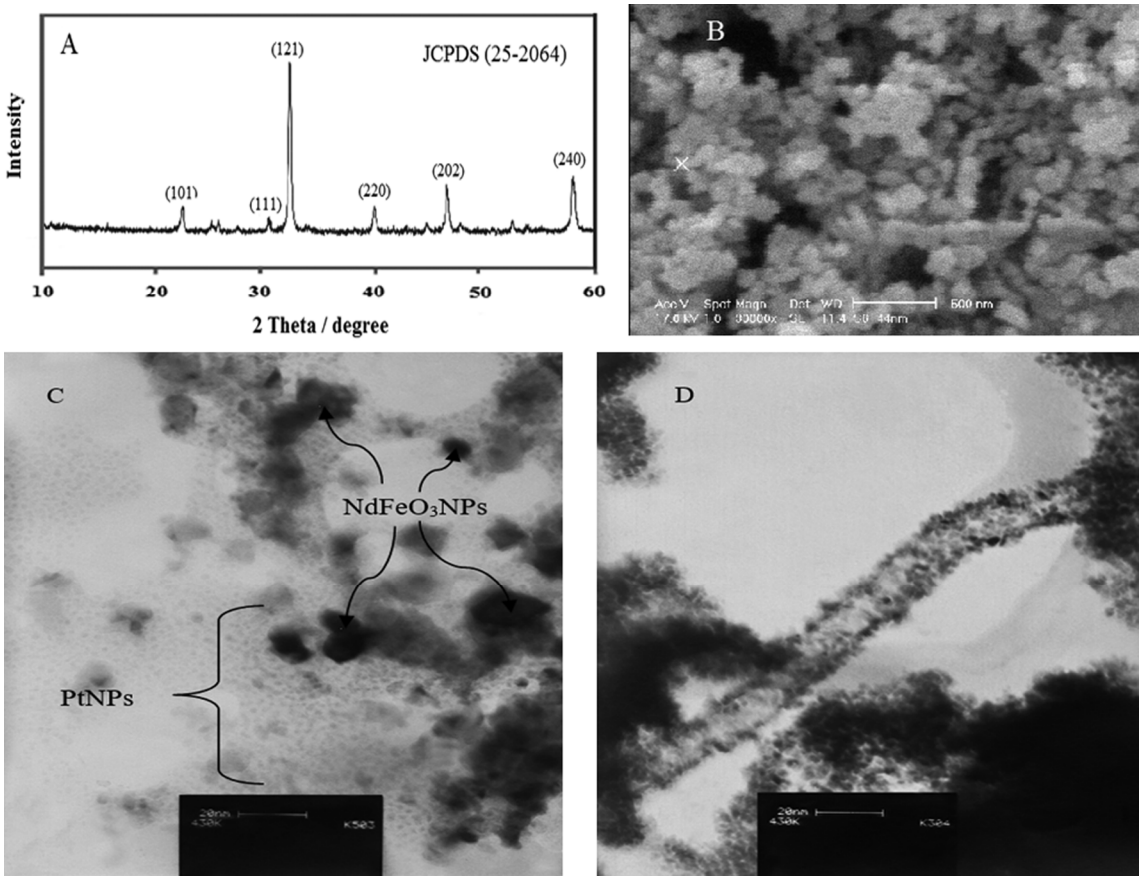

Fig. 1 — (A) XRD and (B) SEM of $NdFeO_3$NPs, (C) TEM image of PtNPs-$NdFeO_3$NPs-CH and (D) TEM image PtNPs-CNTs-CH nanocomposite.

sphere-like $NdFeO_3$NPs obtained were uniform in both morphology and size.

Characterization of PtNPs-CNTs-$NdFeO_3$NPs-CH catalyst

Figure 1C displays the TEM micrograph of the PtNPs-$NdFeO_3$NPs-CH composite. It was realized from Fig. 1C that PtNPs with sizes of 3-10 nm and $NdFeO_3$NPs were uniformly distributed. Figure 1D shows the TEM micrograph of PtNPs-CNTs-CH. It was realized from Fig. 1D that PtNPs well attached to the CNTs and distribute in the surrounding catalyst suspension, also.

Electrochemical behavior of the GC/PtNPs-CNTs-$NdFeO_3$NPs-CH was studied by cyclic voltammetry in 1 M H_2SO_4 at a scan rate of 50mV.s^{-1} with the platinum loading of 0.51 mg.cm^{-2}. As seen in Fig. 2A, the current peaks appeared at-375 mV (c_1) and -250 mV (c_2) in the cathodic and at -290 mV (a_1) and -220 mV (a_2) in the anodic directions are associated with adsorption and desorption of hydrogen on the PtNPs surface. The broad and weak anodic peak at 366mV (a_3) and cathodic peak at 317mV (c_3) are related to the

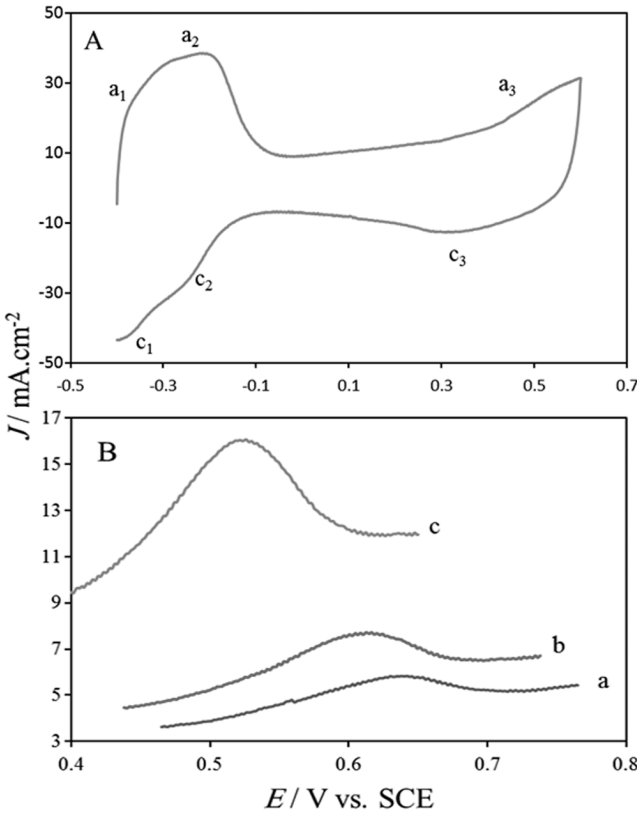

Fig. 2 — (A) Cyclic voltammogram of GC/PtNPs-CNTs-$NdFeO_3$NPs-CH electrode and (B) linear voltammograms of CO stripping (a) GC/PtNPs-CH, (b) GC/PtNPs-$NdFeO_3$NPs-CH and (c) GC/PtNPs-CNTs-$NdFe_2O_3$NPs-CH electrodes in 1M H_2SO_4 at 50mV.s^{-1} scan rate with 0.51 mg.cm^{-2}Pt loading.

formation and reduction of platinum oxides, respectively[22]. The consistent of Fig. 2A voltammogram with the literature[23] confirms the synthesis of platinum nanoparticles properly.

Electrochemical active surface area calculation and accelerated durability test

The electrochemical surface area (EAS) of PtNPs value is an important factor for determination of the catalytic activity, especially for an oxidation reaction as a surface reaction. This parameter can be calculated by cyclic voltammetry techniques. The voltammogram of H_2 adsorption/desorption was used to determine EAS amount of the PtNPs-CNTs-$NdFeO_3$NPs-CH catalyst (Fig. 2A). The platinum EAS of the modified electrodes can be determinate with the calculation of the Columbic charge (Q_H) for hydrogen adsorption/desorption. Q_H is the mean value between the amounts of charge exchanged during the electrochemically adsorption (Q'_H) and desorption (Q''_H) of H_2 on the sites of noble metal[24]:

$$Q_H = \frac{Q'_H + Q''_H}{2} \quad ...(4)$$

It was calculated by determining the area under the peak using SAMA Electroanalyser at the potential rang for the phenomenon of adsorption/desorption of hydrogen on the prepared electrodes. The EAS amount for PtNPs was calculated electrochemically from equation (5) [25]:

$$EAS = \frac{Q_H}{S \times L} \quad ...(5)$$

where L is the PtNPs loading (0.51 mg.cm^{-2}) for the modified electrodes. S = 0.21 is a parameter relating the charge to the area. It represents the charge required for oxidation of a monolayer of H_2 on PtNPs. The EAS of PtNPs-CH,PtNPs-$NdFeO_3$NPs-CH and PtNPs-CNTs-$NdFeO_3$NPs-CH were 11.32, 13.11 and 86.05 $m^2.g^{-1}$, respectively. The perovskite presence at nanocomposite catalyst had a poor effect on hydrogen adsorption/desorption on the catalyst surface. This negligible effect was attributed to Tejuca's study[26]. He expressed that on oxides with Fe ions more oxidized metal centres should be involved in hydrogen adsorption. During the forward scans on catalysts containing perovskite, the current density was raised along the entire investigated potential range[14] that was caused higher EAS for PtNPs-$NdFeO_3$NPs-CH. Perovskites have a wide variety of the structures of surface which affect the surface energy of the mentioned compounds and influence their chemical properties. The relative basicity and acidity of the

atoms present on the surface of the perovskite are affected by the coordination of the metal cation and oxygen anion, which alter the properties of these compounds. For this reason, structural defects in perovskites significantly influence the catalytic properties. The EAS amount for PtNPs-CNTs-$NdFeO_3$NPs-CH catalyst was higher than EAS for PtNPs-CH and PtNPs-$NdFeO_3$NPs-CH catalysts about seven times when compared per same PtNPs mass. This improvement in the electrocatalytic performance of the PtNPs-CNTs-$NdFeO_3$NPs-CH was attributed to the presence of CNTs supports with unique structural and electrical properties that reduced resistances associated with charge exchange[27]. The unique electrical and structural properties of CNTs can be the main parameter for the higher activity in the present study. The high dispersion of the PtNPs on the CNTs supports was achieved with this mechanism: the surface functional groups such as hydroxyl, carboxyl and carbonyl groups on the CNTs were effectively produced during chemical oxidation treatment, and they were assisted ion adsorption and metal deposition by serving as specific nucleation sites for PtNPs[28]. Furthermore, accelerated durability test (ADT) of the nanocatalyst was carried out by applying potentials continuously between -0.4 V and 0.6 V with scan rate 50 $mV.s^{-1}$ in 1 M H_2SO_4 after 100 potential cycles.

$$\%ADT = \frac{(EAS_{run\,1} - EAS_{run\,100})}{EAS_{run\,1}} \times 100 \quad ...(6)$$

The EAS value for the PtNPs-CH catalyst was decreased quickly from 11.32 to 4.89 $m^2.g^{-1}$ after the ADT (about 56.78%), indicating a notable decrease in the PtNPs active surface area. While the EAS value for the PtNPs-$NdFeO_3$NPs-CH catalyst after the ADT has been decreased from13.11 to12.28 $m^2.g^{-1}$ with no significant variation (about 6.31%) indicating no considerable decrease of the PtNPs active surface area at the presence of $NdFeO_3$NPs. Thus, the degradation rate of the PtNPs-$NdFeO_3$NPs-CH catalyst was slower than that of the PtNPs-CH. This is indicated that the PtNPs-$NdFeO_3$NPs-CH catalyst was significantly more durable in the compared to the commercial PtNPs-CH catalyst.

The PtNPs dispersion (D_{Pt}) was termed as the fraction of surface-active atoms of Pt metal in all of atoms of this metal which can be achieved[29]:

$$D_{Pt} = \frac{EAS}{\frac{1}{M_{Pt}} \times (N_A \times 4\pi \times r_{Pt}^2)} \quad ...(7)$$

Where M_{Pt} is the relative Pt molecular weight (195.08 $g.mol^{-1}$), N_A is Avogadro number (6.023×10^{23}) and r_{Pt} is Pt atomic radius (0.139 nm). D_{Pt} of PtNPs-CH,PtNPs-$NdFeO_3$NPs-CH and PtNPs-CNTs-$NdFeO_3$NPs-CH were estimated 0.015, 0.017 and 0.115 $m^2.g^{-1}$, respectively. The PtNPs dispersion on the surface of modified electrodes was improved in the presence of CNTs. The high dispersion of PtNPs on the CNTs as support through the production of uniformly metal particles, in which the functionalized CNTs surface allowed uniform adsorption of the PtNPs produced due to surface functional groups[28].

CO Stripping

For investigation of CO stripping, the linear voltammograms at 50 $mV.s^{-1}$ scan rate were recorded for GC/PtNPs-CH, GC/PtNPs-$NdFeO_3$-CH and GC/PtNPs-CNTs-$NdFeO_3$-CH electrodes. The recorded linear voltammograms of modified electrodes during the reaction of CO oxidation are represented in Fig. 2B. As can be seen from Fig. 2B, there are three considerable differences for CO oxidation on the modified electrodes:

I. The current density of the CO stripping peak was enhanced from 5.80 $mA.cm^{-2}$ for GC/PtNPs-CH electrode to 7.64 and 16.02 $mA.cm^{-2}$ for GC/PtNPs-$NdFeO_3$NPs-CH and GC/PtNPs-CNTs-$NdFeO_3$NPs-CH electrodes, respectively.

II. The peak potential of the CO stripping at GC/PtNPs-CH electrode (= +0.64 V vs. SCE) shifted by 0.02 and 0.12 V to the negative direction compared with that GC/PtNPs-$NdFeO_3$NPs-CH(= +0.62 V vs. SCE) and GC/PtNPs-CNTs-$NdFeO_3$NPs-CH (= +0.52 V vs. SCE) electrode.

III. The $Q_{CO,ads}$ obtained 40.57, 64.92 and 121.97 $C.m^{-2}$ for GC/PtNPs-CH, GC/PtNPs-$NdFeO_3$NPs-CH and GC/PtNPs-CNTs-$NdFeO_3$NPs-CH electrodes, respectively.

The current density increasing of this compound oxidation can be attributed to remove poisoning on the surface nanocatalysts. The lattice oxygen of mixed oxide in $NdFeO_3$ could be considered as active oxygen to remove the CO adsorbed on the noble metal surface. The GC/PtNPs-CNTs-$NdFeO_3$NPs-CH electrode showed better tolerance towards the poisoning through the CO oxidation compared to that of the other modified electrodes.

Methanol oxidation on different modified electrodes

Electrochemical properties of modified electrodes have been investigated by the techniques of electrochemical such as cyclic voltammetry, Anodic Tafel polarization, and Controlled potential coulometry (chronoamperometry) in a known concentration of methanol and 1 M H_2SO_4 aqueous solution.

Cyclic voltammetry

Figure 3A represents cyclic voltammograms of methanol oxidation on different electrodes such as the GC, GC/CH, GC/$NdFeO_3$NPs-CH, GC/PtNPs-CH, GC/PtNPs-$NdFeO_3$NPs-CH and GC/PtNPs-CNTs-$NdFeO_3$NPs-CH in 0.8 M methanol solution and 1 M H_2SO_4 at a scan rate of 50 $mV.s^{-1}$. It is observed that GC and GC/CH electrodes (Fig. 3A, curve a) do not show any peaks for methanol oxidation. It has been known that GC and GC/CH cannot have any catalytic activity for methanol oxidation. The existence of the peak of methanol oxidation for GC/$NdFeO_3$NPs-CH

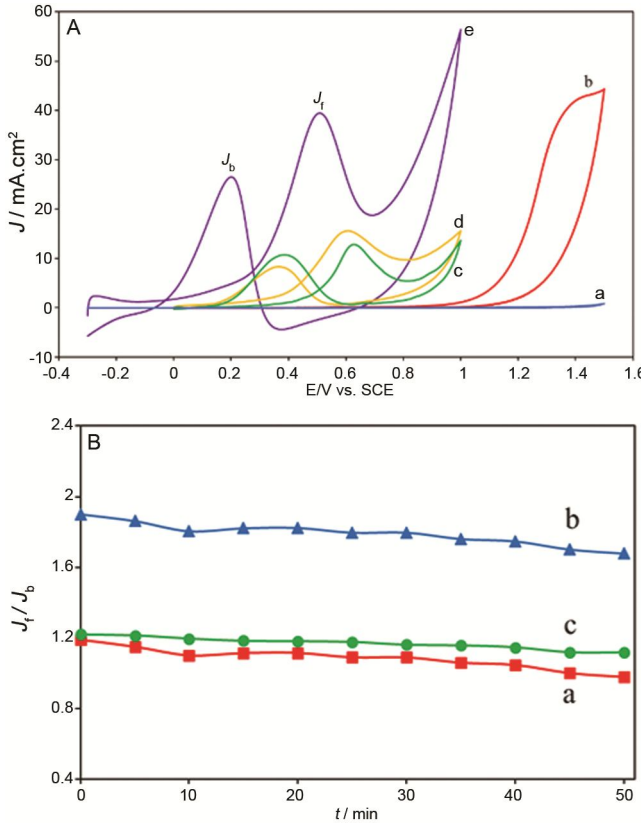

Fig. 3 — (A) CV curves of methanol oxidation on (a) GC and GC/CH, (b) GC/$NdFeO_3$NPs-CH, (c) GC/PtNPs-CH, (d) GC/PtNPs-$NdFeO_3$NPs-CH and (e) GC/PtNPs-CNTs-$NdFeO_3$NPs-CH electrodes and (B) the plot of J_f / J_b ratio as a function of time in 1 M H_2SO_4 and 0.8 M methanol at scan rate of 50 $mV.s^{-1}$.

(Fig. 3A, curve b) was confirmed the catalytic activity of perovskite nanoparticles, but the positive potential peak is not suitable for quick start-up of the fuel cell. It should improve with incorporation the others component to nanocomposite. As seen Fig. 3A curves c to e, two oxidation peaks on Pt-contained electrodes, which were associated with the oxidation of methanol (J_f) and the corresponding produced intermediates (J_b). For comparison of the addition effect of other components on current density and potential, platinum loading (= 0.51 $mg.cm^{-2}$) is similar to different modified electrodes. Table 1 shows the electrochemical data of the cyclic voltammograms on GC/PtNPs-CH, GC/PtNPs-$NdFeO_3$NPs-CH and GC/PtNPs-CNTs-$NdFeO_3$NPs-CH electrodes for methanol oxidation.

The amount of the onset potential for the anodic reaction is important for DMFCs. The decrease in value of the onset potential relates to an improvement in the kinetics of methanol oxidation[30]. According to Table 1, the GC/PtNPs-CNTs-$NdFeO_3$NPs-CH electrode has the lowest value of onset potential. This point shows that the $NdFeO_3$NPs and CNTs incorporation improves the kinetics of reaction and effects on the start-up of fuel cell.

The current density on GC/PtNPs-CNTs-$NdFeO_3$NPs-CH electrode (J_f = 32.24 $mA.cm^{-2}$) is comparable with GC/PtNPs-CH and GC/PtNPs-$NdFeO_3$NPs-CH electrodes (J_f = 12.72 and 15.60 $mA.cm^{-2}$, respectively) and the others containing noble metal or perovskite electrode at similar concentration of methanol as electro-active material[31,32]. These results explain that superior activity for methanol oxidation is corresponded to PtNPs-CNTs-$NdFeO_3$NPs-CH nanocomposites in acidic media.

The currents ratio of the forward and reverse peaks is a parameter to compare the activity of synthetic catalysts for methanol oxidation that is determined as J_f/J_b at Table 1. This ratio is used to determine the tolerance of such catalysts to CO, the intermediate produced during the methanol oxidation. Regarding the larger values as a positive sign, the material synthesized is an excellent CO resistant catalyst[33]. The GC/PtNPs-$NdFeO_3$NPs-CH electrode has the highest value of J_f/J_b ratio (Table 1). The increasing of J_f/J_b ratio was attributed to the removal of CO poisoning on the PtNPs surface by the surface oxygen of the $NdFeO_3$NPs perovskite that was in adjacency of metal particles[34].

Table 1 — Electrochemical data for methanol oxidation on the modified electrodes for 0.8 M methanol in 1M H_2SO_4 at 50mV/s.

Electrode	Onset potential (mV *vs.* SCE)	E_f (mV *vs.* SCE)	J_f (mA.cm^{-2})	E_b (mV *vs.* SCE)	J_b (mA.cm^{-2})	J_f / J_b
GC/PtNPs-CH	50	637	12.72	392	10.73	1.19
GC/PtNPs-$NdFeO_3$NPs-CH	6	608	15.60	378	8.23	1.90
GC/PtNPs-CNTs-$NdFeO_3$NPs-CH	-299	519	32.24	207	26.40	1.22

To examine the poisoning effect of as-prepared electrodes during methanol oxidation reaction, the catalytic activity of mentioned nanocomposites is investigated through cyclic voltammetry repeatedly. Fig. 3B showed the J_f / J_b ratios as a function of time. As observed for GC/PtNPs-CH and GC/PtNPs-$NdFeO_3$NPs-CH electrodes, J_f / J_b is decreased during 50 min, indicating the poor anti-poisoning performance of these catalysts. For GC/PtNPs-CH and GC/PtNPs-$NdFeO_3$NPs-CH electrodes, there is a gradual drop of J_f / J_b ratio within the first 10 min. For GC/PtNPs-CH electrode, the J_f / J_b ratio is stabled during the first 40 min and is gradually decreased after 40 min. PtNPs-$NdFeO_3$NPs-CH catalyst had the highest J_f / J_b ratio after 50 min, indicating that this catalyst is capable of offering excellent anti-poisoning effect toward methanol oxidation reaction. Also, PtNPs-CNTs-$NdFeO_3$NPs-CH catalyst had the stable J_f / J_b ratio for consecutive cycles.

Controlled potential coulometry (chronoamperometry)

The addition effect of functionalized CNTs to PtNPs-$NdFeO_3$NPs-CH nanocomposites on the current density of methanol oxidation was investigated by chronoamperometry technique for a 0.8 M methanol concentration solution (Fig. 4A, solid line). The equations of current density versus time were obtained via the fitting and simulation of experimental data by MATLAB software, and the corresponded curves were plotted in Fig. 4A dash line. As seen in Fig. 4A, there is significant accordance between the experimental data and the fitted curves. The Root Mean Square Error (RMSE) between experimental and fitted plot was calculated by MATLAB software and the plot of RMSE vs. time corresponded to current density on methanol oxidation on the modified electrode is displayed in Fig. 4B. It is clear that the highest and lowest amount of RMSE were related to data for methanol oxidation on GC/PtNPs-CH and GC/PtNPs-CNTs-$NdFeO_3$NPs-CH electrodes, respectively.

In the following, the amount of transferred charge during methanol oxidation versus time was calculated through the lower Riemann sum of curve correspond

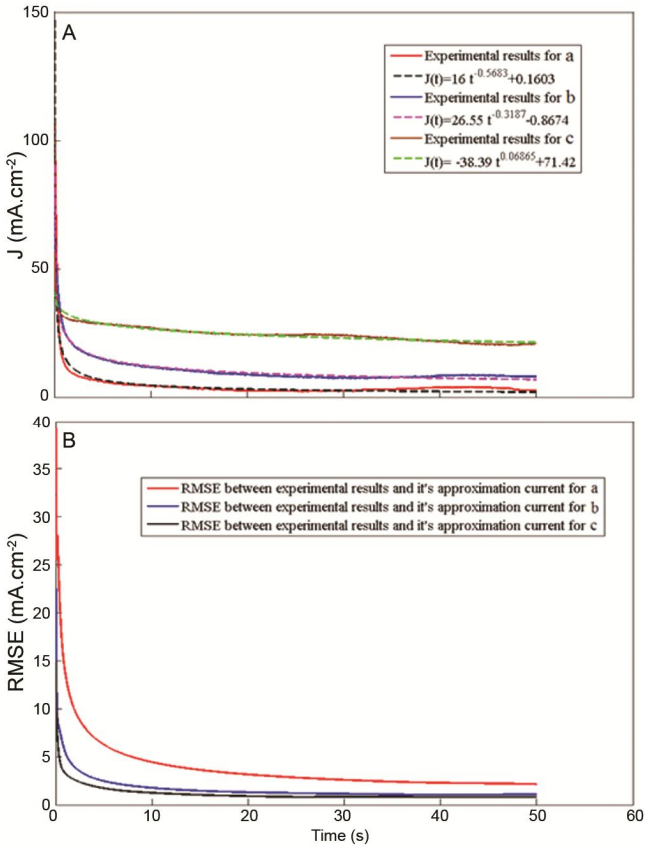

Fig . 4 — (A) The current density vs. time curves on the basis of the experimental and computational data along with fitted equations and (B) the corresponded RMSE for methanol oxidation on the a) GC/PtNPs-CH, b) GC/PtNPs-$NdFeO_3$NPs-CH and c) GC/PtNPs-CNTs-$NdFeO_3$NPs-CH electrodes in 0.8 M methanol and 1 M H_2SO_4 at 0.5 V potential.

to experimental data and the integration of mentioned equations both. The curves of the transferred charge vs. time were plotted for experimental and simulated data (Fig. 5A). By comparing the curves, it is clear that the increasing slope of transferred charge over time is higher for PtNPs-CNTs-$NdFeO_3$NPs-CH than PtNPs-$NdFeO_3$NPs-CH and PtNPs-CH nanocomposites. The plot of RMSE vs. time corresponded to transferred charge on methanol oxidation on the modified electrode is displayed in Fig. 5B. It is clear that the better significant accordance between the experimental data and

the fitted curves was related to the methanol oxidation on GC/PtNPs-CNTs-$NdFeO_3$NPs-CH electrode. Therefore, the composite of CNTs containing showed the higher activity catalytic for methanol oxidation and is a suitable candidate for anodic catalyst in DMFCs. The results of chronoamperometry technique were consistent with the obtained previous consequences of cyclic voltammetry technique.

Anodic Tafel polarization

The intrinsic activity (J_s) of PtNPs-$NdFeO_3$NPs-CH and PtNPs-CNTs-$NdFeO_3$NPs-CH nanocomposites was measured toward the methanol oxidation in 0.8 M methanol and 1 M H_2SO_4 at -1.5 to + 0.5 V vs. SCE in the potential range and the scan rate of 50 $mV.s^{-1}$. The values of the exchange current density (J_0) and polarization resistance (R_p) at Table 2 were obtained by extrapolating the Tafel line to the equilibrium potential (E_{eq}) for the methanol oxidation reaction in 1 M H_2SO_4 solution.

The amount of the Tafel slope was calculated from linear portions of a logarithm of current density *vs.* potential plot ($b \approx 100$ $mV.dec^{-1}$). It was dependent on the coverage of pre-adsorbed CO on the methanol oxidation as anodic reaction[35]. The J_0 value was corrected to the real electrochemical surface area of modified electrodes. The polarization resistance (R_p) could be a criterion for charge exchange on the surface of the anodic catalyst. Giving to table 2, the presence of functionalized CNT in the nanocomposite decreased the R_p value and subsequently enhanced the J_0 amount for GC/PtNPs-CNTs-$NdFeO_3$NPs-CH compared with GC/PtNPs-$NdFeO_3$NPs-CH electrode; which shows that larger exchange current density leads to faster reaction by the aforementioned catalysis.

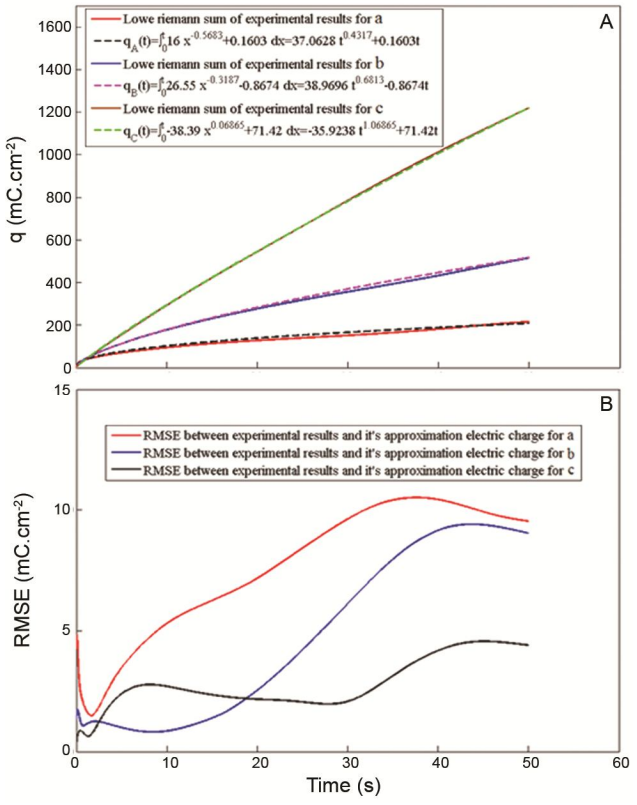

Fig. 5 — (A) The transferred charge vs. time curves on the basis of the experimental and computational data along with fitted equations and (B) the corresponded RMSE during methanol oxidation on the a) GC/PtNPs-CH, b) GC/PtNPs-$NdFeO_3$NPs-CH and c) GC/PtNPs-CNTs-$NdFeO_3$NPs-CH electrodes in 0.8 M methanol and 1 M H_2SO_4 at 0.5 V potential.

Effect of different parameters towards the methanol oxidation on GC/PtNPs-CNTs-$NdFeO_3$NPs-CH electrode

We investigated the methanol oxidation on the GC/PtNPs-CNTs-$NdFeO_3$NPs-CH electrode under the following conditions: methanol concentration, scan rate, and temperature.

Methanol concentration effect and overall reaction order determination

Figure 6A shows the effect of increasing the methanol concentration on the anodic current density and peak potential of methanol oxidation on the GC/PtNPs-CNTs-$NdFeO_3$NPs-CH electrode in 1 M H_2SO_4 at -0.3 to +1 V vs. SCE the potential range and 50 $mV.s^{-1}$ scan rate. It can be observed that increasing the methanol concentration up to 0.95 M increases the anodic current density. The current density of methanol oxidation did not have any considerable increase in methanol concentrations higher than 0.95 M. This effect could be due to the saturation of active sites on the catalyst surface. Moreover, the oxidation reaction of methanol on GC/PtNPs-CNTs-$NdFeO_3$NPs-CH electrode is controlled by the diffusion process of methanol toward catalysis surface. Based on Figure 6A, while the methanol concentration increases, the E_f and E_b shift toward the positive direction. This may be attributed to the poisoning of Pt catalyst when increasing the methanol concentration and the oxidative removal of the adsorbed intermediates which would shift to a more positive potential.

Table 2 — The results of Tafel polarization curve for methanol oxidation on modified electrodes in 0.8 M methanol and 1M H_2SO_4 at 50 mV/s.

Electrode	E_{eq} (mV *vs.* SCE)	J_0 ($mA.cm^{-2}$)	R_p (ohm)
PtNPs-$NdFeO_3$NPs-CH	-0.34	4.93	128.32
PtNPs-CNTs-$NdFeO_3$NPs-CH	-0.47	6.75	102.50

A plot of the logarithm of current density (log *J*) vs. the logarithm of concentration (log *C*) determines the overall order of methanol oxidation reaction[36] using the concentration of methanol in the beginning (Fig. 6B). The reaction order, derived from the slope of the straight line was 0.47 for the positive and 1.38 for the negative sweep.

Scan rate effect and* electron transfer coefficient *determination

For kinetics characterization of methanol oxidation on PtNPs-CNTs-$NdFeO_3$NPs-CH catalyst, the CV curves of methanol oxidation were recorded in 0.8 M methanol and 1 M H_2SO_4 at various sweeping rates in the range of 25-400 $mV.s^{-1}$ on the GC/PtNPs-CNTs-$NdFeO_3$NPs-CH electrode. The plots of the peak potential (E_p) vs. ln (υ) (Fig. 7A) and the anodic peak current density amounts (J) of methanol oxidation vs. the square root of the sweeping rate ($v^{1/2}$) (Fig. 7B) are represented. According to Fig. 7A, the peak potential of methanol oxidation (E_f) was increased with increasing the scan rate, and a linear relationship was obtained between E_f and ln (υ). It shows that the oxidation of methanol is an irreversible process for charge exchange. The plot of E_p and ln (υ) is a straight line with a slope[23]:

$$\frac{\delta E_p}{\delta(\ln \upsilon)} = \frac{R \times T}{(1-\alpha) \times n \times F} \quad ...(8)$$

where α stands for the electron transfer coefficient, describing the effect of electrochemical potential on the activation energy of an electrochemical reaction. The slope of $E_p$vs. ln (υ) was $\delta Ep/\delta(\ln\upsilon)$=44.10 mV. The α value was calculated as 0.90 (giving n = 6 and T=23°C). In operating fuel cells, charge transfer coefficient is the parameter that signifies the fraction of over potential that makes the current density.

It is clear from Fig. 7B that by increasing the applied sweeping rate, the J of methanol oxidation was increased. The linear relationship between the J and $v^{1/2}$ estimate further the control of the overall reaction of methanol oxidation via the mass transport of methanol from the bulk solution to the electrode surface as a result[37].

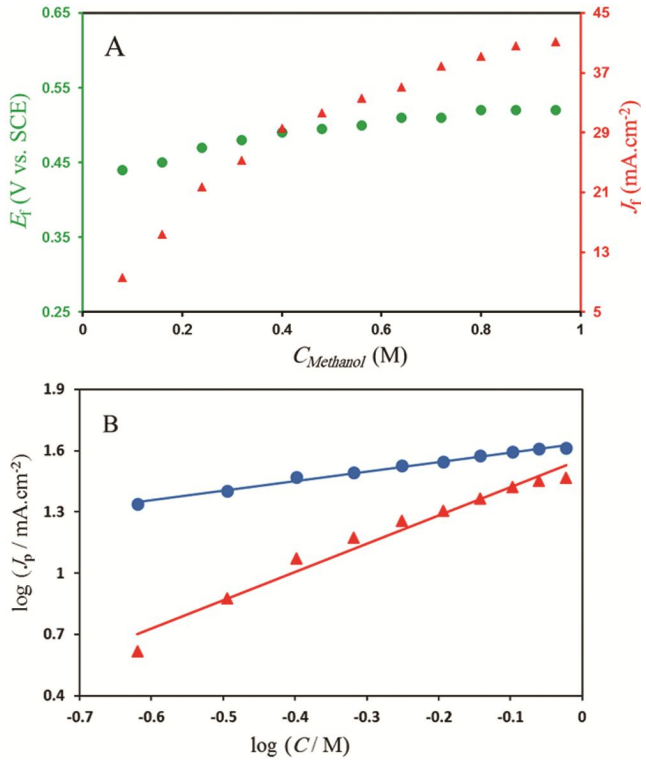

Fig. 6 — Plot of the (A) effect of methanol concentration on peak potential (○) and current density (Δ) of methanol oxidation and (B) peak current dependence *vs.* the logarithm of methanol concentration on the GC/PtNPs-CNTs-$NdFeO_3$NPs-CHelectrode in 1 M H_2SO_4 at -0.3 to +1 V *vs.* SCE the potential range and 50 $mV.s^{-1}$ scan rate.

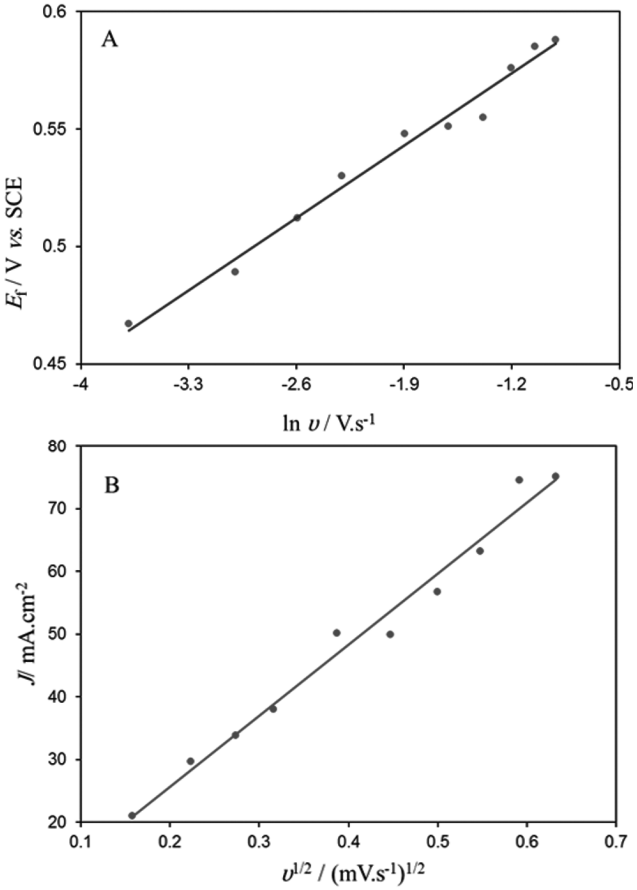

Fig. 7 — The plots of (A) the anodic peak potential *vs.* ln υ and (B) the anodic peak current density of methanol oxidation *vs.*$\upsilon^{1/2}$ on the GC/PtNPs-CNTs-$NdFeO_3$NPs-CH electrode in 0.8 M methanol and 1 M H_2SO_4 at different scan rates: 25 - 400 $mV.s^{-1}$.

Temperature effect and activation energy determination

The electrochemical activity of GC/PtNPs-CNTs-$NdFeO_3$NPs-CH electrode towards the methanol oxidation was investigated at temperature levels ranging from 23 to 80°C and the CV curves are reported at Fig 8A. When the temperature was changed from 23 to 80°C, the *J* was increased from 37.38 to 244.70 $mA.cm^{-2}$ with an increment factor of more than 6.5. Therefore, mass transport becomes an important factor for higher activity. At the same methanol concentration, the upper current density indicated that the fine structures of the catalyst possess more available PtNPs active sites to participate in the electrochemical reaction of methanol oxidation. The relatively higher incremental factor of the *J* with temperature increase verifies that the very good 3D interconnection in CNTs and the highly ordered pores could provide PtNPs-CNTs-$NdFeO_3$NPs-CH with easier mass transport and subsequently superior efficiency, which suggests that the carbon compounds with ordered structure are suitable for the use as catalyst support materials in DMFCs[38]. The activation energy of methanol oxidation was determined by studying reaction at different temperatures between 23 and 80°C on GC/PtNPs-CNTs-$NdFeO_3$NPs-CH electrode. Arrhenius plots of logarithm of transferred current density (log J_p) *vs.* the reciprocal of temperature (T^{-1}) provided the activation energy from the slope of linear fitted as displayed in Fig. 8B. The Activation energy was calculated from the changes slope of the Arrhenius plot for certain potential values by applying the equation (9)[39]:

$$\frac{\partial \ln J_p}{\partial\left(\frac{1}{T}\right)} = \frac{Ea}{R} \qquad ...(9)$$

The apparent activation energy of methanol at GC/PtNPs-CNTs-$NdFeO_3$NPs-CH electrode was 31.5 $kJ.mol^{-1}$.

Mechanism of methanol oxidation on PtNPs-$NdFeO_3$NPs-CH nanocomposite

Similar to the mechanism of methanol oxidation on the surface of noble metal like platinum[40], it seems that the possible reaction pathway is as follows:

$$Pt + CH_3OH \rightarrow Pt\text{-}(CO)_{ads} + 4H^+ + 4e^- \qquad ...(10)$$

$$Pt\text{-}(CO)_{ads} + H_2O \rightarrow Pt + CO_2 + 2H^+ + 2e^- \qquad ...(11)$$

It seems that the possible reaction pathway of methanol oxidation on the perovskite $NdFeO_3$ surface in the presence of an acidic electrolyte be as follows (M^{n+}: $Nd^{2+}$and Fe^{3+}):

$$O^{2-}\text{—}M^{n+}\text{—}O^{2-} + H_2O \rightarrow O^{2-}\text{—}M^{n+}.H_2O_{ads}\text{—}O^{2-} \qquad ...(12)$$

$$O^{2-}\text{—}M^{n+}.H_2O_{ads}\text{—}O^{2-} + H_2O \rightarrow O^{2-}\text{—}M^{n+}.OH^-_{ads}\text{—}O^{2-} + H_3O^+ \qquad ...(13)$$

$$O^{2-}\text{—}M^{n+}.OH^-_{ads}\text{—}O^{2-} \rightarrow O^{2-}\text{—}M^{(n+1)+}.OH^-_{ads}\text{—}O^{2-} + e^- \qquad ...(14)$$

In the following:

$$O^{2-}\text{—}M^{(n+1)+}.OH^-_{ads}\text{—}O^{2-} + CH_3OH \rightarrow O^{2-}\text{—}M^{(n+1)+}.OCH_3^-{}_{ads}\text{—}O^{2-} + H_2O \qquad ...(15)$$

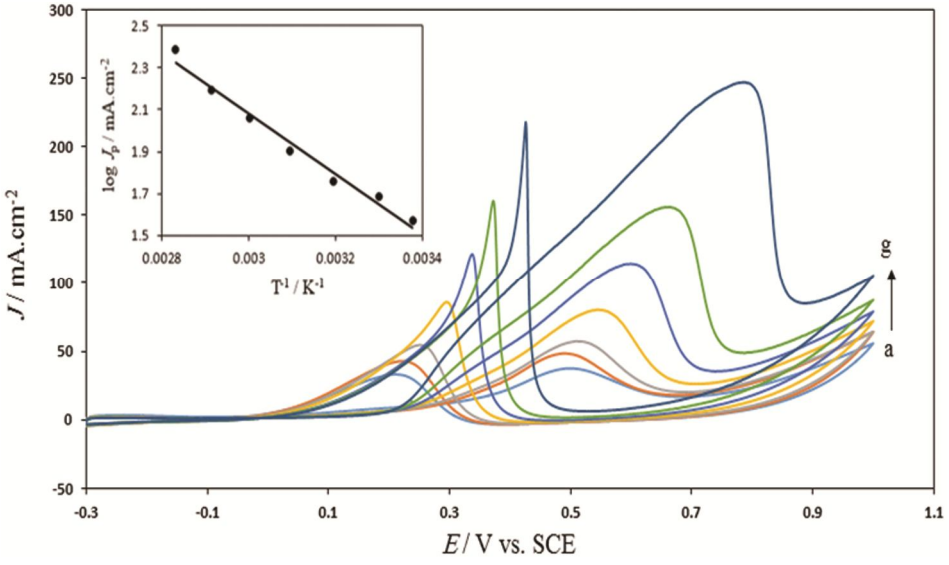

Fig. 8 — Cyclic voltammograms of methanol oxidation at different temperatures: a) 23, b) 30, c) 40, d) 50, e) 60, f) 70 and g) 80°C. Inset: Arrhenius plot for the determination of activation energy of methanol oxidation on GC/PtNPs-CNTs-$NdFeO_3$NPs-CH in 0.8 M methanol and 1M H_2SO_4.

$$O^{2-}—M^{(n+1)+}.OCH_3^-{}_{ads}—O^{2-} + 3H_2O \rightarrow O^{2-}—M^{(n+1)+}.OC_{ads}—O^{2-} + 3H_3O^+ + 4e^- \quad ...(16)$$

$$O^{2-}—M^{(n+1)+}.OC_{ads}—O^{2-} \rightarrow O^{2-}—M^{(n+1)+}— + CO_2 + 2e^- \quad ...(17)$$

$$O^{2-}—M^{(n+1)+}— + 3H_2O \rightarrow O^{2-}—M^{(n+1)+}—O^{2-} + 2H_3O^+ \quad ...(18)$$

$$O^{2-}—M^{(n+1)+}—O^{2-} + 2H_2O \rightarrow O^{2-}—M^{(n+1)+}.OH^-{}_{ads}—O^{2-} + H_3O^+ \quad ...(19)$$

$$O^{2-}—M^{(n+1)+}.OH^-{}_{ads}—O^{2-} + CH_3OH + 5H_2O \rightarrow O^{2-}—M^{(n+1)+}.OH^-{}_{ads}—O^{2-} + CO_2 + H_2O + 6H_3O^+ + 6e^- \quad ...(20)$$

Schematic 1 display the oxidation of methanol molecule on the electrode surface containing perovskite. Based on the suggested mechanism, the catalytic activity of the nanoparticles toward methanol oxidation was affected by both the absorption of methanol molecule along with the electrical and oxygen ion conductivities of perovskite. The presence of transition metal ions improved the oxidation of methanol. It is clear that the metals with the higher oxidation number have more power for oxidizing of methanol. The surface oxygen of the $NdFeO_3$ nanoparticles in adjacency of metal particles removed the CO poisoning on the surface of the platinum nanoparticles. Metal hydroxides formed during hydrolysis can be reduced to metal nanoparticles.

Single cell performances

To investigate the improved performance of the 2.0% PtNPs- 0.6% CNTs-1.0% $NdFeO_3$NPs-CHcatalyst (Pt-CNT-$NdFeO_3$NPs-CH/CC-DL), single cell tests were carried out for the MEA made as the anode and the PtNPs-CH (4 mg.cm^{-2}) catalyst as the cathode for CH_3OH/O_2. The performance of the proposed single cell system depends on the efficiency of the electrochemical reaction at the interface between the solid phase of the electrode surface and liquid and gas phases in anode and cathode sides, the temperature of the fuel cell and methanol concentration of carrier stream has major effects and has to be optimized.

To study the temperature effect on the performance of the fuel cell, various temperatures ranging from 60-90°C were tested while keeping [methanol] constant at 1M with a flow rate of 1.43 ml.min^{-1} and [P_{O_2}] = 2 bar. The results have been shown in Fig. 9A. From the *I-V* characteristics, maximum power density of the single cells using the Pt-CNT-$NdFeO_3$NPs-CH/CC-DL anode was obtained at 90°C. The OCV of single cells were obtained between 0.4 V for fuel cell temperature ranging from 60-90°C. It is observed that the increasing of temperature was caused the enhancing of DMFC power density. It can be due to the faster kinetics of methanol oxidation and oxygen reduction at the higher temperature.

The methanol concentration as fuel can have a significant effect on electrical performances of single cell such as cell voltage and power density, as one would expect. The polarization curves of the single cell system were obtained for various methanol concentrations. Figure 9B shows the results for PtNPs-CNTs-$NdFeO_3$NPs-CH catalyst in the DMFC as an anode in 1, 2 and 3 M methanol concentrations. The power density was enhanced with

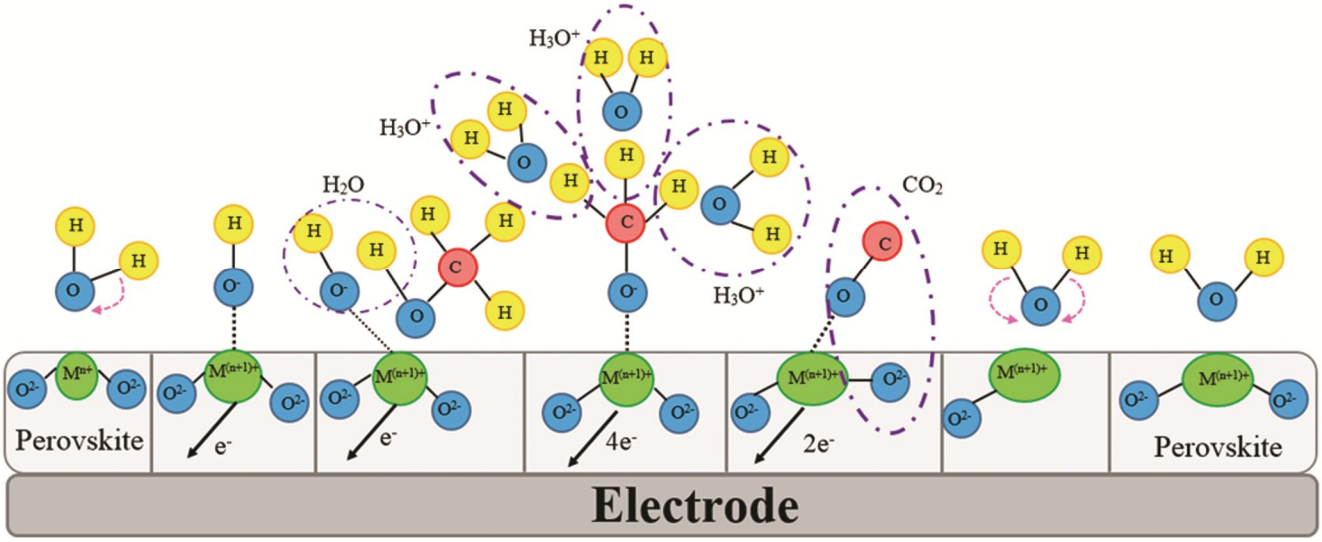

Scheme 1 — Mechanism of methanol oxidation on the electrode surface containing perovskite.

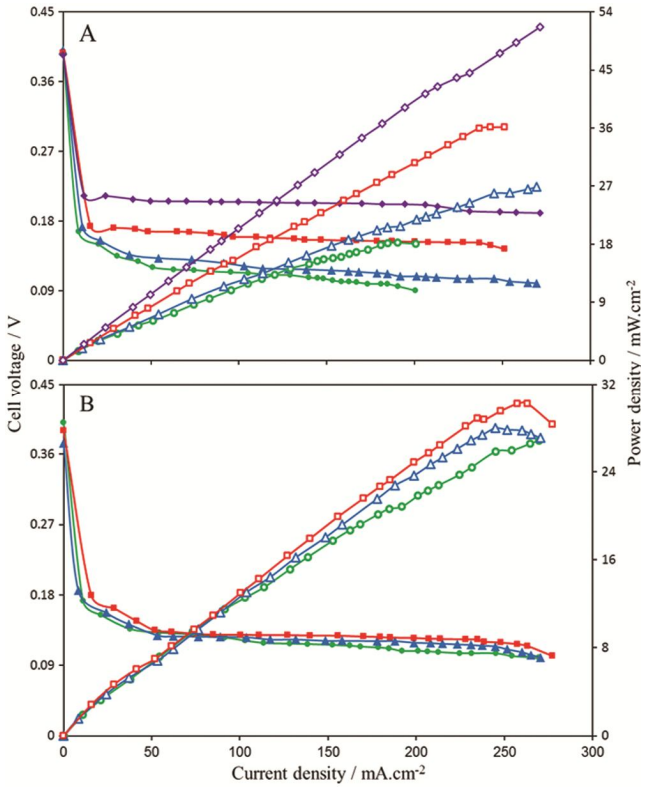

Fig. 9 — Electrical performances (Cell voltage against current density and power density against current density) of a 5 cm^2 DMFC at different (A) temperature (○) 60, (Δ) 70, (□) 80 and (◊)90°C and (B) methanol concentrations (○) 1, (Δ) 2 and (□)3 M using the Pt-CNT- $NdFeO_3$NPs-CH/CC-DL anode (P_{O_2}= 2 bar; flow rate = 1.43 $mL.min^{-1}$ and Nafion® 117 membrane).

concentration increasing of methanol as a fuel that it can be due to the large number and desaturation of catalytic sites.

Conclusion

Effectively, PtNPs-$NdFeO_3$NPs-CH and PtNPs-CNTs-$NdFeO_3$NPs-CH nanocomposites have been synthesized. GC/PtNPs-CNTs-$NdFeO_3$NPs-CH electrode was proposed as active catalysts for methanol oxidation. Our results showed that the addition of $NdFeO_3$NPs and CNTs into PtNPs catalyst matrix and the use of a more porous matrix of CH could considerably advance the electrode performance for methanol oxidation in DMFcs. The transition metals presence (Nd and Fe) at catalyst structure was caused to catalyze the methanol dehydrogenation. The lessening the poisoning rate of the PtNPs with intermediates and by-products of anodic reaction were observed due to the multifunctional effect electrical and oxygen ion conductive perovskite. The activity of PtNPs-CNTs-$NdFeO_3$NPs-CH composite for methanol oxidation was higher than that of PtNPs-CH and PtNPs-$NdFeO_3$NPs-CH according to the anodic peak potential and onset potential of methanol oxidation. The reason PtNPs utilization in the methanol oxidation reaction was intrinsically related to PtNPs formation but using $NdFeO_3$NPs increased the DMFCs performance with low Pt loading.

Acknowledgement

This work was supported by University of Sistan and Baluchestan (USB) for financial support.

References

1 Guo D J, Cui Sh K & Sun H, *J Nanopart Res*, 11 (2009) 707.
2 Li Z, Ji Sh, Pollet B G & Shen P K, *J Nanopart Res*, 15 (2013) 1959.
3 Li L, Chen M, Huang G, Yang N, Zhang L, Wang H, Liu Y, Wang W & Gao J, *J Power Source*, 263 (2014) 13.
4 Bai Zh, Shi M, Niu L, Li Zh, Jiang L & Yang L, *J Nanopart Res*, 15 (2013) 2061.
5 Singh R N, Sharma T, Singh A, Anindita, Mishra D & Tiwari S K, *Electrochim Acta*, 53 (2008) 2322.
6 Augustin C O, Berchmans L J & Selvan R K, *Mater Lett*, 58 (2004) 1260.
7 Porta P, Cimino S, Rossi S D, Faticanti M, Minelli G & Pettiti I, *Mater Chem Physic*, 71 (2001)165.
8 Simner S P, Bonnett J F, Canfield N L, Meinhardt K D, Shelton J P, Sprenkle V L & Stevenson J W, *J Power Sources*, 113 (2003) 1.
9 Liang M, Yu B, Wen M, Chen J, Xu J & Zhai Y, *J Power Sources*, 190(2009) 341.
10 Bartolomeo E D, Traversa E, Baroncini M, Kotzeva V & Kumar R V, *J Eur Ceram Soc*, 20 (2000) 2691.
11 Alifanti M, Kirchnerova J & Delmon B, *Appl Catal A Gen*, 245 (2003) 231.
12 Spinicci R, Faticanti M, Marini P, De Rossi S & Porta P, *J Mol Catal A Chem*, 197 (2003) 147.
13 Khanfekr A, Arzani K, Nemati A & Hosseini M, *Int J Environ Sci Tech*, 6 (2009) 105.
14 Deshpande K, Mukasyan A & Varma A, *J Power Sources*, 158 (2006) 60.
15 Chen T, Shen L, Liu F, Zhu W, Zhang Q & Chu X, *J Rare Earth*, 30 (2012) 1138.
16 Figueiredo J L, Pereira M F R, Serp P, Kalck P, Samant P V& Fernandes J B, *Carbon*, 44 (2006) 2516.
17 Mukherjee S, Bates A, Lee S C, Lee D H & Park S, *Int Jou Green Energy* , 12 (2015) 787.
18 Ekrami-Kakhki M S, Khorasani-Motlagh M & Noroozifar M, *J Appl Electrochem* , 41 (2011) 527.
19 Khaleghian-Moghadam R, Noroozifar M, Khorasani-Motlagh M & Ekrami-Kakhki M S, *J Solid State Electrochem* , 11 (2012) 643.
20 Khorasani-Motlagh M, Noroozifar M, Yousefi M & Jahani Sh, *Int J Nanosci Nanotech*, 9 (2013) 7.
21 Noroozifar M, Khorasani-Motlagh M & Yavari Z, *Int J Nanosci Nanotech*, 9 (2013) 85.
22 Razmi H, Habibi Es & Heidari H, *Electrochim Acta*, 53 (2008) 8178.

23 Tong H, Li H L & Zhang XG, *Carbon*, 45 (2007) 2424.
24 Rao C V, Singh S K & Viswanathan B, *Indian J Chem B*, 47 (2008) 1619.
25 Saha M S, Li R & Sun X, *J Power Sources*, 177 (2008) 314.
26 Tejuca LG, *Thermochim Acta*, 126 (1988) 205.
27 Li W, Liang C, Zhou W, Qiu L, Zhenhua, Sun G & Xin Q, *J Physic Chem B*, 107 (2003) 62929.
28 Seo M H, Choi S M, Kim H J, Kim J H, Cho B K & Kim W B, *J Power Sources*, 179 (2008) 81.
29 Chen Y, Bai L, Zhou C, Lee J M & Yang Y,*Chem Commun*, 47 (2011) 6452.
30 Barakat NAM, Motlak M, Kim B S, El-Deen A G, Al-Deyab S S & Hamza AM, *J Mol Catal A Chem*, 394 (2014) 177.
31 Xu Y & Lin X, *Electrochim Acta*, 52 (2007) 5140.
32 Léger J M, *Electrochim Acta*, 50 (2005) 3123.
33 Raghuveer V, Thampi K R, Xanthopoulos N, Mathieu H J & Viswanathan B, *Solid State Ionics*, 140 (2001) 263.
34 Rajesh T & Devi R N, *J Mol Catal A Chem*, 395 (2014) 534.
35 Jiang J & Aulich T, *J Power Sources*, 209 (2012) 189.
36 Becerık İ, Sūzer Ş & Kadirgan F, *J Electroanal Chem*, 502 (2001) 118.
37 Guo DJ & Li HL, *J Power Sources*, 160 (2006) 44.
38 Song S, Liang Y, Li Z, Wang Y, Fu R, Wu D & Tsiakaras P, *Appl Catal B Environ* 98 (2010) 132.
39 Yavari Z, Noroozifar M & Khorasani-Motlagh M, *J Appl Electrochem*, 45 (2015) 439.
40 Alcaide F, Álvarez G, Cabot PL, Grande HJ, Miguel O & Querejeta A, *Int J Hydrogen Energy*, 36 (2011) 443